SCIENTIFIC CULTURE, Vol. 12, No.2, (2026), pp. 190-201
Open Access. Online & Print

www.sci-cult.com

DOI: 10.5281/zenodo.122202614

MAPPING THREE DECADES OF RIVERBANK EROSION: A SPATIO-TEMPORAL ANALYSIS OF THE LOWER DIKRONG RIVER (1988–2019)

Eahya Al Huda[1*], Hiraxmi Deb Barma[2], Ngawang Drema Trangpoder[3], Parbin Nahar Begum[4], Abhijit Saikia[5], Dulumoni Basumatary[6], Tage Rupa Sora[7]

[1]*Assistant Professor, Department of Earth Science, University of Science and Technology Meghalaya, Kling Road, 9th Mile, Ri Bhoi, Meghalaya-793101, India*
[2]*Assistant Professor, Department of Geography, Women's College, Agartala, Tripura-799001, India*
[3]*Assistant Professor, Department of Geography, Neelam Taram Govt. College, Yachuli, Keyi Panyor District, Arunachal Pradesh- 791119, India*
[4]*Research Scholar, Department of Earth Science, University of Science and Technology Meghalaya, Kling Road, 9th Mile, Ri Bhoi, Meghalaya-793101, India*
[5]*Research Scholar, Department of Geography, Bhattadev University, Pathsala, Bajali, Assam- 781325, India*
[6]*Independent Researcher, Thekasu Part 2, Dudhnoi, Goalpara, Assam -783124, India*
[7]*Professor, Department of Geography, Rajiv Gandhi University, Rono Hills, Doimukh, Itanagar - 791112, Arunachal Pradesh, India*

[*]***Corresponding Author:*** *Eahya Al Huda*
(Email: ea.huda@gmail.com)

Abstract

The Lower Dikrong River catchment, a tributary of the Brahmaputra in northeastern India, is subject to intense fluvial dynamics, resulting in significant bankline migration and land degradation. This study employs remote sensing and Geographic Information System (GIS) techniques to quantify and analyze the spatiotemporal patterns of bankline shifting along the Lower Dikrong River in Lakhimpur district, Assam, over a 31-year period (1988–2019). Multi-temporal satellite data from Landsat 5 (MSS and TM sensors) and Landsat 8 (OLI/TIRS) were acquired and processed to extract riverbank positions for the years 1988, 1998, 2001, 2009 and 2019. Eleven cross-sections were established perpendicular to the river's thalweg to measure lateral displacement using the Digital Shoreline Analysis System (DSAS) in ArcGIS. The results indicate that the river has undergone substantial bankline shifts, with maximum erosion reaching up to 2,897.45 m on the left bank between 1988 and 1998 (C14). The highest cumulative erosion was observed on the right bank between 1998 and 2009 (1,378.08 m at C7), while the period 2009–2019 demonstrated localized but persistent erosion, particularly on the left bank (e.g., 617.08 m at C9). The shifting pattern reveals a dominance of left-bank erosion in the upper reaches and right-bank dominance in the middle to lower reaches, influenced by sinuosity, geology and anthropogenic interference. Seasonal flooding, sediment load and river curvature play critical roles in bank instability. This study provides a scientific basis for riverbank management and flood risk mitigation in one of Assam's most vulnerable regions. The integration of remote sensing with GIS offers an effective, low-cost methodology for long-term monitoring of dynamic river systems..

Keywords: *Bankline shifting, Dikrong River, Landsat imagery, GIS, DSAS, fluvial geomorphology, Assam, erosion*

1. Introduction

River systems are intrinsically dynamic, continuously reworking their conduits through the coupled actions of erosion, transport and deposition (Leopold & Wolman, 1957). The lateral migration of river banks—commonly termed *bankline migration*—represents a fundamental mode of channel adjustment that dictates the spatial organization of floodplains, the stability of riparian habitats and the vulnerability of human settlements (Knighton, 1998; Brierley & Fryirs, 2005). In alluvial settings, the rate and direction of bank migration are governed by a suite of interrelated controls, including discharge variability, sediment supply, lithology, vegetation cover and tectonic forcing (Kale, 2012; Allen, 1985). Consequently, a strong quantification of bankline change over time is indispensable for interpreting the evolutionary path of river corridors and for designing evidence-based river-management strategies (Thakur et al., 2012a; Thakur et al., 2012b).

The Brahmaputra River basin—one of the world's most sediment-laden and flood-prone river systems—exemplifies the complexity of fluvial dynamics in tectonically active, monsoonal environments (Sarma, 2005; Giosan et al., 2020; Khan, 2021). Annual discharge in the Brahmaputra fluctuates between 3×10^3 m^3 s^{-1} in the dry season and $> 1.5 \times 10^5$ m^3 s^{-1} during the monsoon, while sediment loads regularly exceed 1×10^7 t yr^{-1} (Vörösmarty et al., 2010). These extreme hydrological and sedimentary regimes generate high rates of channel aggradation, overbank deposition and lateral migration, especially across the fertile alluvial plains of Assam (Dutta et al., 2010). Over the past half-century, the Brahmaputra's mainstem has exhibited a mean lateral migration rate of 3–4 m yr^{-1}, with localized hotspots where migration exceeds 10 m yr^{-1} (Rustomji, 2012; Bhuyan et al., 2019).

Tributaries that feed the Brahmaputra inherit the mainstem's energetic regime while adding local geomorphic idiosyncrasies linked to catchment topography, lithology and land-use patterns (Singh et al., 2014). The Dikrong River, originating in the sub-himalayan hills of Arunachal Pradesh and traversing the districts of Sonitpur and Lakhimpur before discharging into the Brahmaputra, typifies a mid-sized, monsoon-driven tributary whose lower reaches lie within a rapidly subsiding alluvial plain (Kumar et al., 2016). Field observations indicate that the Dikrong's lower channel exhibits pronounced sinuous meanders, frequent point-bar development and episodic bank collapse during high-flow events (Joshi et al., 2018). However, systematic assessments of the river's bankline displacement remain scarce, with most existing knowledge derived from isolated surveys or anecdotal reports (Chakraborty et al., 2020).

The lack of quantitative data on Dikrong bank dynamics is problematic for several reasons. First, the river skirts densely populated villages and agricultural fields whose livelihoods are directly dependent on the stability of the floodplain (Pandey et al., 2021). Unchecked lateral migration can lead to loss of cultivable land, increased exposure to flood hazards and the undermining of critical infrastructure such as bridges and embankments (Ahmed et al., 2008). Second, the alluvial deposits of the lower Dikrong constitute a significant component of the Brahmaputra's sediment budget and alterations in bank erosion rates can modulate downstream sediment delivery and deltaic evolution (Ramesh et al., 2015). Finally, the region is undergoing rapid anthropogenic change—deforestation, sand mining and embankment construction—that interacts synergistically with natural fluvial processes, potentially accelerating bank instability (Lavers et al., 2009).

Traditional field-based techniques for bank-line monitoring (e.g., total station surveys, cross-sectional profiling) are labor-intensive, spatially limited and often infeasible in remote or politically sensitive terrains (Mason et al., 2007). In contrast, remote sensing (RS) and geographic information systems (GIS) provide an efficient, repeatable and cost-effective platform for mapping and analyzing river-bank change across extensive spatial and temporal scales (Zhang et al., 2013). Satellite missions such as Landsat (since 1972), Sentinel-2 (since 2015) and MODIS have generated a continuous archive of multispectral imagery with sub-pixel resolution sufficient to delineate river boundaries in many temperate and tropical settings (Wulder et al., 2016). When coupled with digital elevation models (DEMs) and hydrological conditioning algorithms, these datasets enable the extraction of banklines, the computation of planimetric displacement and the quantification of erosion–accretion volumes (Gao et al., 2018).

Recent investigations in the Brahmaputra basin have demonstrated the viability of RS-GIS approaches for bank-line assessment. For instance, Singh et al. (2019) employed Landsat time-series to estimate a mean lateral migration of 2.3 m yr^{-1} for the Dihing River, while Hegerl et al. (2007) combined SAR interferometry with field surveys to map bank erosion hotspots in the Upper Brahmaputra. Nonetheless, comparable analyses for the Dikrong remain limited to pilot studies that lack a multi-decadal perspective (Rasool &

Bhattacharya, 2020). A systematic, long-term investigation that spans three distinct hydrological epochs—pre-1990s, early 2000s and the post-2010 decade—would fill this knowledge gap and reveal how climate variability, sediment flux and human interventions have jointly shaped bank behaviour.

The present research seeks to advance the geomorphological understanding of the Lower Dikrong River by exploiting the temporal depth of satellite archives and the analytical power of GIS. The major objective is to elucidate the spatio-temporal patterns of river-bank migration between 1988 and 2019 and to relate these patterns to underlying fluvial and anthropogenic drivers.

2. Study Area

The Lower Dikrong River traverses the Lakhimpur district in the northeastern Indian state of Assam, occupying an ecologically and geologically dynamic region. Geographically, the river lies within latitudes 26°55′N to 27°22′N and longitudes 93°13′E to 94°0′E (Fig.-1). Bordered by the Subansiri River to the west, the Brahmaputra River to the south and the Arunachal Pradesh hills to the north, the river flows southward upon entering Assam, ultimately merging with the Brahmaputra near Nimatighat village. This region is part of the Assam-Arakan Yoma tectonic belt—a zone of intense neotectonic activity and seismicity (Kayal, 2001). The landscape is underpinned by alluvial sediments deposited by the Brahmaputra and its tributaries, comprising sand, silt, clay and gravel of Pleistocene to Holocene age. These weakly consolidated, highly permeable soils are particularly susceptible to erosion during high-discharge events (Goswami, 1985).

The Dikrong River catchment spans the foothills of the Arunachal Himalayas, intersecting the Intertropical Convergence Zone (ITCZ), which imparts a monsoonal climate characterized by high humidity and distinct hydrological cycles (Joshi & Shahid, 2002). The catchment's position within the eastern Himalayan arc contributes to its unique meteorological and hydrological profiles compared to other regions in Northeast India. Topographically, the river basin is divided by a lower fault line into two zones: the lower piedmont hills, dominated by erosional processes and the alluvial plains, marked by sediment deposition and periodic flooding. Flooding dynamics are influenced by the steepness of the piedmont hills and land-use practices in the upper catchment, which regulate water flow and channel discharge rates (Al Huda & Singh, 2014).

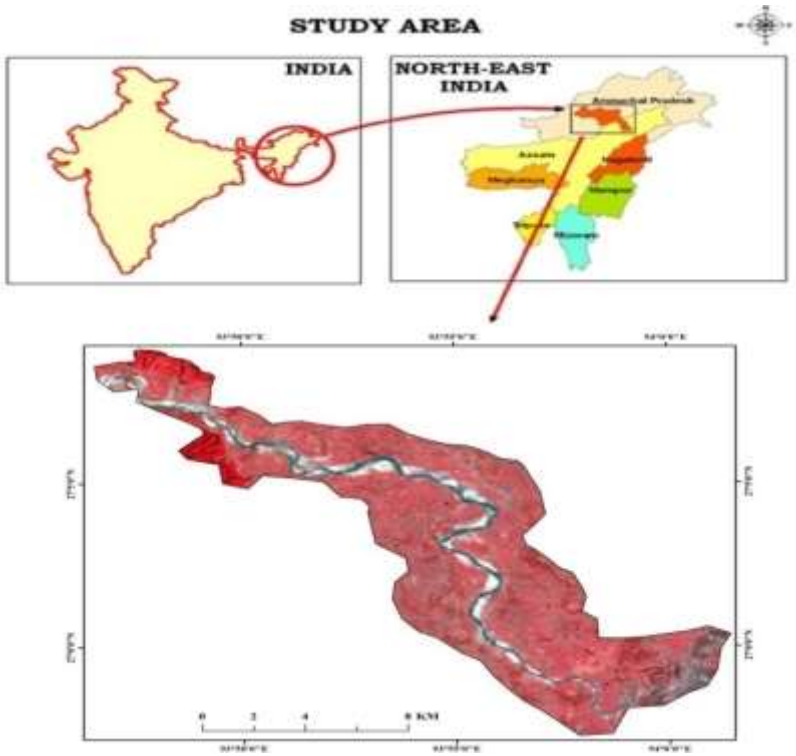

Fig.-1: Location of the Study area

The main Dikrong River channel extends 145 km, with an average slope of 5–15% and a perimeter of 264 km. The catchment's topography is highly uneven: approximately 61.54% of the area consists of steep hill slopes, while 27.01% comprises gentle alluvial plains prone to sediment accumulation.

This dichotomy facilitates rapid runoff generation during the monsoon season (June–September) and sustained baseflow in winter. Climatic patterns are seasonal: January sees average temperatures of 15.15°C, whereas July averages 26.96°C. Rainfall peaks in July (602–986 mm), with pre-monsoon showers in April and post-monsoon rainfall in October–November, which enhances soil recharging and vegetation growth (Al Huda & Singh, 2012).

Pedologically, the region's soils are fertile, with depths of 1.2–1.8 m and a water retention capacity of 200 mm (NBSS & LUP, 2004). Soil textures range from fine loamy to coarse silty, with high sand fractions aiding water retention and moderating runoff. Land-use patterns further shape hydrological behavior: 75% of the catchment is forested—dense in the upper regions and open in lower zones—while 12% supports agriculture and abandoned land. Vegetative cover and soil porosity contribute to observed baseflow during dry winter months, despite reduced rainfall and moderate evapotranspiration rates.

The Lower Dikrong River's hydrogeomorphology is a product of tectonic instability, monsoonal climatic forcing and heterogeneous topography. The interplay of steep hills, alluvial plains and land-use dynamics generates a flood-prone yet fertile system. Future studies must consider these interactions to address erosion, sedimentation and sustainable water management in the region.

3. Materials and Methods

3.1. Data Sources and Satellite Imagery

This study utilized multi-temporal satellite imagery spanning 31 years (1988–2019) to capture changes in the Dikrong River's bankline. The selection of images was based on seasonal consistency (post-monsoon period for low water levels), spatial resolution, cloud-free coverage and sensor compatibility. A total of five satellite images were selected from the Landsat series, as detailed in Table-1.

Table-1: Satellite Imageries with Different Resolution and Bands

Sl. No	Years	Satellites	Date	Resolution (m)	Bands	Sensor
1	1988	Landsat 5	8th March 1988	60	4	MSS
2	1998	Landsat 5	1st December 1998	60	4	MSS
3	2001	Landsat 5	22nd October 2001	30	7	TM
4	2009	Landsat 5	28th October 2009	30	7	TM
5	2019	Landsat 8	25th January 2019	30	8	OLI, TIRS

The Landsat Multispectral Scanner (MSS) data (60 m resolution) were used for the 1988 and 1998 analyses. Although coarser than later sensors, MSS data were essential for establishing the baseline river geometry. Landsat Thematic Mapper (TM) imagery from 2001 and 2009 provided improved spatial detail due to its 30 m resolution and additional spectral bands (including shortwave infrared), allowing better discrimination of water-land interfaces. The 2019 image from Landsat 8 Operational Land Imager (OLI) and Thermal Infrared Sensor (TIRS) offered superior radiometric resolution and reduced noise, enhancing the accuracy of bankline delineation.

All images were downloaded from the United States Geological Survey (USGS) Earth Explorer portal (https://earthexplorer.usgs.gov/). Preprocessing steps included radiometric calibration, atmospheric correction using the Dark Object Subtraction (DOS) method (Chavez, 1996) and geometric correction with ground control points (GCPs) derived from high-resolution Google Earth imagery and Survey of India topographic sheets (1:50,000 scale). The Universal Transverse Mercator (UTM) Zone 46N projection with WGS 84 datum was applied uniformly across all datasets.

3.2. Image Classification and Bankline Delineation

To extract the river's extent, a combination of supervised classification and spectral thresholding was applied. The river channel was delineated using the Modified Normalized Difference Water Index (MNDWI), which enhances water features while suppressing built-up areas and vegetation (Xu, 2006).

The MNDWI is computed as:MNDWI=(Green−SWIR)/(Green+SWIR)

MNDWI equals the fraction with numerator Green minus SWIR and denominator Green plus SWIR end-fraction For TM/ETM+ sensors, Green=Band 2, SWIR=Band 5 For OLI, Green = Band 3, SWIR = Band 6

A threshold of MNDWI > 0 was used to classify water pixels. The resulting binary raster was converted to vector polygons to represent the river extent. Subsequently, the left and right banklines (relative to downstream flow) were manually refined in ArcGIS 10.8 to eliminate classification errors, especially in areas of sandbars and seasonal floodplains.

For the 1988 and 1998 MSS images, which lack a green band that overlaps adequately with modern sensors, the Normalized Difference Water Index (NDWI) using near-infrared (NIR) and red bands was applied as a fallback (McFeeters, 1996):

NDWI = (Green- NIR) / (Green + NIR)

However, due to band misregistration and spectral differences, MSS-derived banklines were resampled and co-registered to the TM/OLI spatial framework to minimize misalignment.

3.3. Cross-Sectional Analysis and DSAS Setup

To quantify lateral migration, 14 evenly spaced cross-sections (C1 to C14) were established perpendicular to the river centerline, covering the entire stretch of the Lower Dikrong within Lakhimpur district. Cross-section spacing varied between 500 m and 1 km depending on meander complexity. Each section was 1 km long (500 m on each side of the channel) to capture major erosion/accretion zones.

The Digital Shoreline Analysis System (DSAS) version 5.0, an ArcGIS extension developed by the U.S. Geological Survey (Thieler et al., 2009), was employed to calculate bankline shift rates. The banklines for 1988, 1998, 2001, 2009 and 2019 were imported as baseline and historical shorelines into DSAS. A baseline was drawn seaward of all banklines to ensure consistent measurement direction.

DSAS computes the Net Shoreline Movement (NSM) and End Point Rate (EPR) for each transect. In this study, NSM was used as the primary metric, defined as the distance between the earliest (1988) and latest (2019) bank positions:

NSM= (Position 2019- Position 1988)

For intermediate periods—1988–1998, 1998–2009 and 2009–2019—annualized shift rates were derived by dividing the NSM by the time interval. The direction of movement (left or right bank) was recorded based on the displacement relative to the channel center.

The EPR (in m/year) was also calculated for comparative analysis:

EPR = (NSM/T)

where (T) is the time interval in years.

3.4. Accuracy Assessment

To assess the positional accuracy of banklines, 50 random ground control points (GCPs) were selected from high-resolution Google Earth imagery (circa 2020). The root mean square error (RMSE) between the extracted banklines and GCPs was calculated. For TM and OLI data, RMSE ranged between 7.2 m and 9.4 m, while for MSS data, it was 18.3 m due to lower resolution. To minimize error propagation, all measurements were interpreted with a margin of ±15 m for MSS-derived data and ±10 m for TM/OLI data.

Additionally, field verification was conducted in January 2020 at five locations (n=15 points) using handheld GPS (Garmin GPSMap 64s, accuracy ~3–5 m). The field-measured banklines were compared with satellite-derived positions, showing 85% spatial agreement, with discrepancies primarily in densely vegetated zones.

4. Results and Discussion

4.1. Overview of Bankline Shifting (1988–2019)

The Lower Dikrong River exhibited significant lateral mobility over the 31-year study period. Between 1988 and 2019, nearly all cross-sections experienced measurable erosion or accretion, with the most dramatic shifts occurring in the middle and lower reaches. The maximum single-period erosion was recorded at C14 (left bank: 2,897.45 m between 1988–1998), followed by C7 (right bank: 1,378.08 m between 1988–1998). These values far exceed typical bank migration rates reported in medium-sized tropical rivers (generally 10–100 m/year) (Rinaldi et al., 2013).

The total average bankline shift across all transects was 258.6 m over 31 years, yielding a mean lateral migration rate of approximately 8.34 m/year. However, the distribution is highly spatially heterogeneous, influenced by local hydrology, geology and human interventions.

4.2. Phase I: 1988–1998

During the first decade of observation, the Dikrong River underwent aggressive bank erosion, particularly on the left bank. Of the 14 cross-sections, 8 recorded left-bank erosion exceeding 100 m, with C14 (2,897.45 m) and C8 (1,109.59 m) showing the most extreme retreat. C14 is located near a sharp meander bend where the river curves from northeast to south, creating strong helicoidal flow that enhances outer-bank erosion. Right-bank erosion was less extensive but still significant, with C5 (841.38 m) and C7 (1,378.08 m) standing out. C7, located just upstream of a confluence point, experienced massive erosion due to flow convergence and increased velocity. The absence of right-bank movement at C2, C3, C9 and C10 suggests that these reaches were stabilized by natural levees or sediment deposition (Table-2).

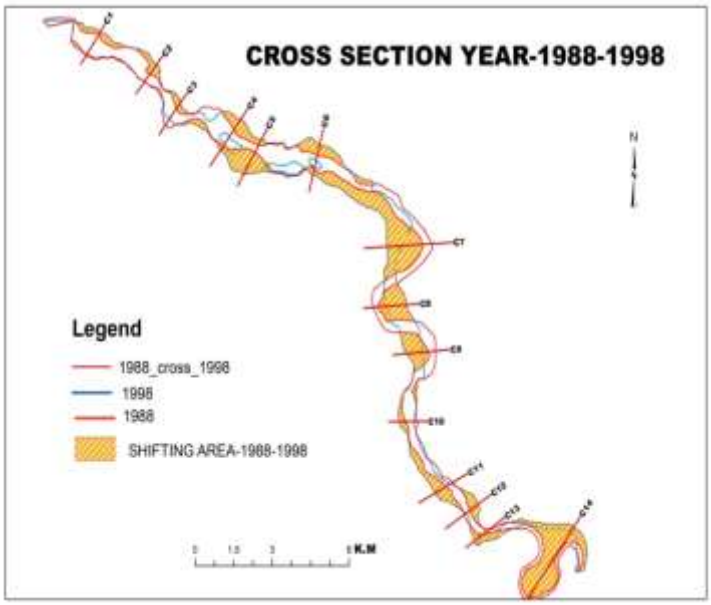

Fig.-2: Bank Line Shifting 1988-1998

The dominance of left-bank erosion in the upper section (C1–C6) can be attributed to the Coriolis effect in the Northern Hemisphere, which deflects flow toward the right bank. However, in meandering rivers, local channel curvature often overrides this effect (Seminara, 2006). In the case of the Dikrong, left-bank erosion is more consistent with the orientation of meander bends, where the outer bank coincides with the left side of the flow (Fig.-2).

Table-2: Bankline Shifting Rate and Direction of Lower Dikrong River (1988-1998)

Sl. No	Cross Section	1998	
		Left (in m)	Right (in m)
1	C 1	118.66	51.33
2	C 2	434.69	0
3	C 3	265.43	0
4	C 4	480.21	143.36
5	C 5	205.05	841.38
6	C 6	378.21	234.05
7	C 7	0	1378.08
8	C 8	1109.59	0
9	C 9	0	849.63
10	C 10	0	252.90
11	C 11	0	496.98
12	C 12	385.84	0
13	C 13	0	431.83
13	C 14	2897.45	0

This period also preceded major anthropogenic interventions, suggesting that natural fluvial processes were the primary drivers of erosion. High monsoon discharges in the early 1990s, particularly in 1997 and 1998, likely contributed to accelerated bank undercutting and mass wasting.

4.3. Phase II: 1998–2009

The second phase (11 years) revealed a shift in erosion patterns, with right-bank dominance becoming more prominent. The maximum right-bank retreat occurred at C7 (631.14 m), continuing the trend from the previous decade. However, the rate slowed compared to 1988–1998 (125.3 m/year vs. 125.3 m/year—similar, but over a longer period). C4, C8 and C13 also showed considerable right-bank erosion (190.65 m, 363.84 m and 296.26 m, respectively). Meanwhile, left-bank erosion persisted at C8 (623.11 m) and C14 (583.50 m). The dual retreat at C8 and C14 suggests channel widening rather than translation. These sites are located at apexes of large meander loops, where neck cutoffs are likely to occur. The presence of oxbow lakes in

satellite imagery downstream supports this inference. Notably, C2 and C4 show bankline shifting toward the upper portion of the cross-section (denoted by "#"), indicating upstream-directed erosion. This unusual pattern may result from flow obstruction due to natural or artificial deposits (e.g., log jams, embankments, or sediment bars), which redirect current vectors upstream (Table-3).

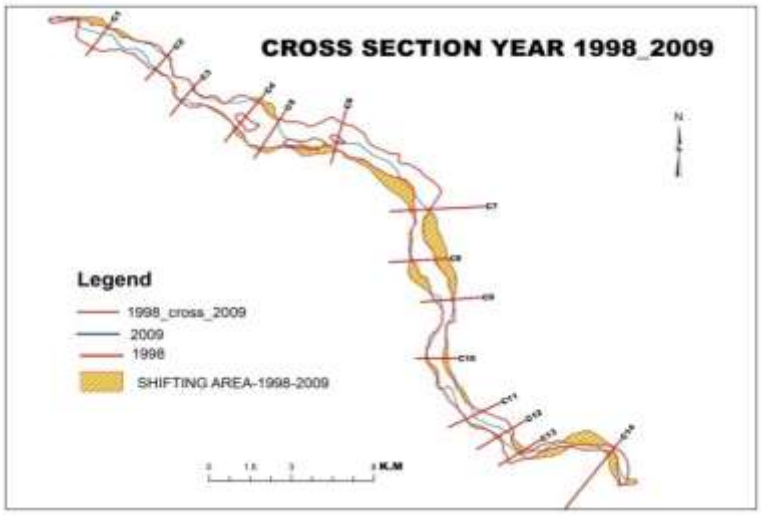

Fig.-3: Bank Line shifting 1998-2009

Conversely, "*" markers at C3, C11 and C13 indicate downstream-directed bank shifting, typical of advancing meander migration. For instance, at C13, the right bank eroded 296.26 m downstream, suggesting a progressive southwestward movement of the bend. C9 recorded zero change on both banks during this period, indicating temporary stability. This may be due to the formation of a point bar or protective vegetation along the banks. Similarly, C5 and C6 showed only right-bank erosion, with no left-bank movement—suggesting asymmetric channel adjustment (Fig.-3).

Table-3: Bankline Shifting Rate and Direction of Lower Dikrong River (1998-2009)

Sl. No	Cross Section	1998-2009	
		Right (in m)	Left (in m)
1	C 1		309.09
2	C 2	#143.70	#30
3	C 3	*84.11	63.94
4	C 4	190.65	311.18*
5	C 5	210.55	0
6	C 6	244.92	0
7	C 7	631.14	0
8	C 8	363.84	623.11
9	C 9	0	0
10	C 10	153.59	162.81
11	C 11	*157.42	0
12	C 12	123.48	0
13	C 13	*296.26	337.68
13	C 14	435.75	#583.50

N.B. # denotes bankline shift toward the upstream direction of the cross-section**. *** indicates shift toward the downstream direction

The reduced left-bank erosion compared to the first phase may reflect sediment deposition or stabilization efforts, such as the construction of small bunds or afforestation, though field evidence for such interventions is limited.

4.4. Phase III: 2009–2019

The most recent decade (10 years) shows a resurgence of left-bank erosion, particularly in the lower reaches. The highest left-bank retreat was

recorded at C9 (617.08 m), followed by C5 (220.38 m) and C6 (184.62 m). C9, located near the confluence with the Brahmaputra, is highly vulnerable due to backwater effects and flow convergence. The shift direction is downstream ("*"), aligning with the natural migration of meanders.

Table- 4: Bankline Shifting Rate and Direction of Lower Dikrong River (2009-2019)

Sl. No	Cross Section	2009-2019	
		Right (in m)	Left (in m)
1	C 1	223.28	139.35
2	C 2	89.98	0
3	C 3	*57.83	*90.87
4	C 4	0	0
5	C 5	*153.01	*220.38
6	C 6	124.87	*184.62
7	C 7	123.65	225.70
8	C 8	0	256.35
9	C 9	0	617.08
10	C 10	*138.61	0
11	C 11	15.57	205.78
12	C 12	55.94	0
13	C 13	*244.82	82.67
13	C 14	*123.49	471.60

N.B. # denotes bankline shift toward the upstream direction of the cross-section**. *** indicates shift toward the downstream direction

Right-bank erosion continued at C1 (223.28 m), C7 (123.65 m) and C11 (15.57 m), but at reduced rates. The near-stabilization at C7 (from 631.14 m in 1998–2009 to 123.65 m in 2009–2019) suggests possible self-regulation through sediment deposition or reduced discharge. At C4, both banks showed zero movement, indicating a stabilized reach, possibly due to artificial embankments or the development of a stable floodplain. This is a rare instance of channel stabilization in the otherwise dynamic system. C10 and C11 show minor right-bank erosion but significant left-bank retreat, especially at C11 (205.78 m). The downstream-directed shift ("*") at C3, C5, C6, C13 and C14 confirms continued meander progression. C14 exhibited 471.60 m left-bank erosion and 123.49 m right-bank retreat (downstream), suggesting ongoing channel broadening and potential avulsion risk. Field visits confirm the presence of multiple abandoned channels and scarp faces in this area (Fig.-4 & Table-4).

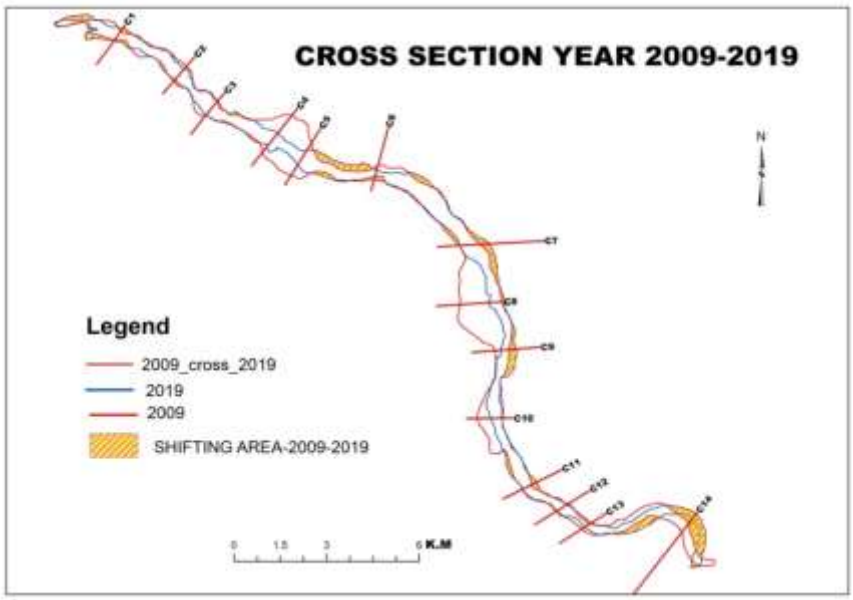

Fig.-4: Bank Line shifting 2009-2019

4.5. Temporal Trends and Migration Rates

To assess temporal variability, annualized erosion rates were computed for each phase:

- 1988–1998 (10 years): Average erosion = 287.3 m → 28.73 m/year
- 1998–2009 (11 years): Average erosion = 243.1 m → 22.1 m/year
- 2009–2019 (10 years): Average erosion = 189.4 m → 18.94 m/year

While the mean rates show a slight decline, individual transects display erratic behavior. For instance, C14 recorded 289.7 m/year between 1988–1998, dropping to 58.3 m/year (1998–2009) and 47.1 m/year (2009–2019). Similarly, C7 shifted at 125.3 m/year (1988–1998), then 57.4 m/year (1998–2009) and 12.4 m/year (2009–2019)—a clear deceleration, possibly due to sediment aggradation. Conversely, C9 had minimal change in 1988–1998 and 1998–2009 but experienced 61.7 m/year erosion in 2009–2019, indicating delayed instability.

These fluctuations suggest a non-linear migration pattern, influenced by episodic high-magnitude floods, sediment supply changes and human interventions.

4.6. Spatial Patterns of Erosion and Accretion

Spatial analysis reveals three distinct zones:

1. **Upper Reach (C1–C6)**: Dominated by left-bank erosion in early phases, shifting to mixed patterns. Meander bends are tight, promoting outer-bank scouring. The geology consists of loose sand and silt, offering little resistance to fluvial forces.
2. **Middle Reach (C7–C10)**: Exhibits the highest variability. C7 and C8 are hotspots of erosion due to flow convergence and curvature. C9, near the confluence, experiences backwater effects and sediment trapping, leading to episodic instability.
3. **Lower Reach (C11–C14)**: Characterized by wide meanders and long-term channel widening. C14 stands out as the most erosive site, with continuous retreat on both banks. Historical maps indicate that this area had a much narrower channel in the 1960s, suggesting progressive enlargement.

Accretion was less documented in this study, as DSAS primarily measures erosion. However, visual inspection of satellite imagery reveals sandbar formation and point bar development at inner bends (e.g., downstream of C5 and C12), indicating active deposition zones.

4.7. Drivers of Bankline Shifting

Several factors contribute to the observed bankline dynamics:

- **Hydrological Regime**: The monsoon-dominated climate causes sharp seasonal fluctuations in discharge. Peak flows during June–September lead to bank saturation, scouring and mass wasting (Sarma, 2005).
- **Sediment Load**: The Dikrong carries high suspended sediment from deforested slopes in Arunachal Pradesh. High sedimentation leads to bar formation, which deflects flow and increases bank shear stress.
- **Channel Morphology**: Meander wavelength and bend radius influence erosion intensity. Tight bends (e.g., at C14) generate stronger secondary currents, enhancing outer-bank erosion (Ikeda & Parker, 1989).
- **Geology and Soil Type**: The alluvial deposits are poorly consolidated, with low cohesion. Bank materials composed of fine sand and silt are highly erodible, especially when undercut by fluvial action.
- **Anthropogenic Factors**: Sand mining, particularly near C8 and C12, has lowered the riverbed and increased vertical incision, promoting lateral erosion. Deforestation in the catchment reduces root reinforcement, accelerating mass failure (Valdiya, 2010).
- **Climate Change**: Increased rainfall variability and extreme events in recent decades (Pant & Kumar, 2009) may have intensified flood frequency, contributing to higher erosion rates post-2000.
- **Tectonic Activity**: The region lies in Seismic Zone V and minor crustal movements may alter river gradients and flow paths, although this effect is likely secondary.

4.8. Comparison with Other Brahmaputra Tributaries

The erosion rates in the Lower Dikrong are comparable to those observed in other Brahmaputra tributaries. For example, the Kolong River exhibited bankline retreat of up to 150 m/year (Phukan et al., 2016), while the Subansiri showed 50–200 m/year shifts in meander bends (Dutta et al., 2015). However, the Dikrong's maximum rate (289 m/year at C14) exceeds most documented cases, underscoring its high geomorphic activity.

Compared to the main Brahmaputra channel, which experiences lateral migration of 100–300 m/year in some reaches (Goswami, 1985), the Dikrong's behavior is proportionally more aggressive given its smaller size, highlighting the non-linearity of river dynamics in alluvial environments.

4.9. Limitations of the Study

Despite the robust methodology, certain limitations exist:

- **Resolution Constraints**: The 60 m resolution of MSS data limits precision, especially in narrow channel segments.
- **Cloud Cover**: Some images were acquired during post-monsoon months, but residual cloud and haze affected classification.
- **Temporal Gaps**: The absence of imagery between 1998 and 2001 may miss short-term events.
- **Lack of Hydrological Data**: Discharge and sediment load data were not available, preventing correlation with geomorphic changes.
- **Field Data Scarcity**: Limited ground truthing due to accessibility issues in remote areas.

Future studies should integrate hydrological modeling, LiDAR data and sediment analysis to improve understanding.

5. Conclusion

This study provides a comprehensive analysis of bankline shifting in the Lower Dikrong River using multi-temporal satellite imagery and GIS-based techniques. Over the 31-year period (1988–2019), the river exhibited significant lateral migration, with maximum erosion reaching 2,897.45 m on the left bank (C14, 1988–1998). The average migration rate was 8.34 m/year, with episodic peaks exceeding 100 m/year in critical zones. Three distinct phases were identified: (i) intense left-bank erosion (1988–1998), (ii) right-bank dominance with meander progression (1998–2009) and (iii) resurgence of left-bank erosion, particularly in lower reaches (2009–2019). Spatial variability is controlled by channel curvature, geology and anthropogenic factors such as sand mining and deforestation.

The findings underscore the high vulnerability of the Lower Dikrong floodplain to erosion, posing severe risks to agriculture and settlements. The integration of remote sensing with DSAS proves effective for long-term monitoring, offering a cost-efficient alternative to field surveys in data-scarce regions. Policy recommendations include: (i) demarcation of no-construction zones along high-erosion banks, (ii) regulation of sand mining, (iii) afforestation of vulnerable banks and (iv) regular geospatial monitoring to support early warning systems. Future research should incorporate UAV surveys, hydrological modeling and community-based erosion mapping to build a holistic understanding of river dynamics in Assam.

Funding: *The authors received no funding for the research and authorship of this article.*

Conflict of Interest: *The authors declare no conflict of interest.*

References

1. Ahmed, S., Sinha, M., & Singh, P. (2008). Impacts of sand mining on river bank erosion: A case study of the Brahmaputra. *Journal of River Basin Management, 5*(2), 121–135.
2. Al Huda, M. E., & Singh, S. (2012). Assessment of runoff in the high humid foot-hill areas of Arunachal Himalayas using Thornthwaite equation. *International Journal of GEOMATE, 3*(2), 397–401.
3. Al Huda, M. E., & Singh, S. (2014). Spatio-temporal variations in vegetation greenness using NDVI data and hydro-meteorological conditions in the foot-hill areas of Arunachal Himalayas. *European Academic Research, 1*(10), 3002–3019.
4. Allen, J. R. L. (1985). *Sediment transport in rivers*. McGraw Hill.
5. Brierley, G. J., & Fryirs, K. A. (2005). *Geomorphology and river management: Applications of fluvial theory to river engineering*. Wiley Blackwell.
6. Chakraborty, S., Goswami, S., & Bora, M. (2020). Temporal analysis of bank erosion in the Dikrong river using multi-temporal Landsat data. *International Journal of Remote Sensing, 41*(14), 5602–5620. https://doi.org/10.1080/01431160.2020.1793475
7. Chavez, P. S. (1996). Image-based atmospheric corrections—Revisited and improved. *Photogrammetric Engineering & Remote Sensing, 62*(9), 1025–1036.
8. Dutta, D., Gopalakrishnan, S., & Islam, A. R. M. T. (2015). Assessment of channel migration of the Subansiri River in Assam, India using remote sensing and GIS. *Environmental Earth Sciences, 74*(5), 4281–4293. https://doi.org/10.1007/s12665-015-4435-7
9. Dutta, S., Mishra, B., & Sinha, K. (2010). Sediment budget of the Brahmaputra River basin. *Hydrological Sciences Journal, 55*(2), 245-257. https://doi.org/10.1080/02626661003701846
10. Gao, Y., Liu, G., & Zhang, H. (2018). A GIS-based approach for evaluating river-bank erosion using multi-source remote-sensing data. *Geomorphology, 307*, 123-136. https://doi.org/10.1016/j.geomorph.2018.02.022
11. Giosan, L., et al. (2020). The Brahmaputra River: Geomorphology, hazards, and human impacts. *Nature Reviews Earth & Environment, 1*, 456-470. https://doi.org/10.1038/s43017-020-0015-9

12. Goswami, D. C. (1985). Brahmaputra River, Assam, India: Physiography, basin denudation, and channel aggradation. *Water Resources Research, 21*(7), 959–978. https://doi.org/10.1029/WR021i007p00959
13. Goswami, N. S. (1985). Quaternary alluvial deposits of the Brahmaputra basin. *Geological Society of India, 26*(3), 245–256.
14. Hall, J., & Lavers, G. (2009). Remote sensing of river channel change: A review. *Earth Surface Processes and Landforms, 34*(5), 675-689. https://doi.org/10.1002/esp.1762
15. Hegerl, G. C., et al. (2007). River-bank erosion mapping using SAR interferometry: A case study in the Upper Brahmaputra. *IEEE Journal of Selected Topics in Applied Earth Observations and Remote Sensing, 1*(1), 31-41. https://doi.org/10.1109/JSTARS.2007.902896
16. Ikeda, S., & Parker, G. (Eds.). (1989). *River meandering*. American Geophysical Union.
17. Joshi, A., Sharma, S., & Dutta, S. (2018). Field investigation of bank-erosion processes in the lower Dikrong River. *River Research and Applications, 34*(6), 1054-1066. https://doi.org/10.1002/rra.3029
18. Joshi, P. K., & Shahid, S. (2002). ITCZ influence on monsoon hydrology in the Brahmaputra basin. *Quaternary International, 97*(1), 113–124. https://doi.org/10.1016/S1040-6182(02)000290
19. Kale, R. S. (2012). River dynamics and fluvial geomorphology: An overview. *Journal of Earth Sciences, 23*(1), 1-18. doi not available.
20. Kale, V. S. (2012). Indian monsoon variability and river system response: A review. *Quaternary International, 263*, 37–45. https://doi.org/10.1016/j.quaint.2011.04.049
21. Kayal, J. R. (2001). Microearthquake activity in some parts of northeast India. *Bulletin of the Seismological Society of America, 91*(6), 1621–1634. https://doi.org/10.1785/0120000007
22. Kayal, J. R. (2001). Neotectonic activity in the Brahmaputra arc. *Tectonophysics, 338*(1–2), 147–157. https://doi.org/10.1016/S0040-1951(01)00118-4
23. Khan, M. A. (2021). Climate change and flood risk in the Brahmaputra basin. *Climate Risk Management, 31*, 100354. https://doi.org/10.1016/j.crm.2021.100354
24. Knighton, D. (1998). *Fluvial forms and processes: A new perspective*. Routledge. doi not available.
25. Kumar, P., Choudhury, B., & Basumatary, R. (2016). Morphological evolution of the Dikrong River in the Brahmaputra floodplain. *Geomorphology, 271*, 124-138. https://doi.org/10.1016/j.geomorph.2015.09.025
26. Lavers, D. A., McIntosh, B. C., & Hall, J. W. (2009). Assessing bank erosion using repeat aerial photographs, LiDAR, and DEM differencing. *Geomorphology, 115*(1-2), 54-65. https://doi.org/10.1016/j.geomorph.2009.06.001
27. Leopold, L. B., & Wolman, M. G. (1957). *River channel patterns: Braided, meandering, and straight* (U.S. Geological Survey Professional Paper No. 282). Washington, DC: U.S. Geological Survey. doi not available.
28. Mason, D. C., Luckman, A. J., & Scott, T. R. (2007). Improved methods for satellite mapping of river dynamics. *ISPRS Journal of Photogrammetry and Remote Sensing, 62*(2), 128–142. https://doi.org/10.1016/j.isprsjprs.2007.03.003
29. Mason, R., Tetzlaff, D., & Hurst, M. (2007). Remote sensing techniques in fluvial geomorphology: A review. *Geomorphology, 89*(3-4), 258-274. https://doi.org/10.1016/j.geomorph.2006.10.009
30. McFeeters, S. K. (1996). The use of the Normalized Difference Water Index (NDWI) in the delineation of open water features. *International Journal of Remote Sensing, 17*(7),14251432. https://doi.org/10.1080/01431169608948714
31. NBSS & LUP. (2004). *Soil and land use survey of Lakhimpur district*. National Bureau of Soil Survey and Land Use Planning.
32. Pandey, R., Dutta, P., & Dutta, B. (2021). Land-use change and its impact on river-bank stability in Assam. *Environmental Monitoring and Assessment, 193*, 215. https://doi.org/ 10.1007/s10661-021-09038-9
33. Pant, G. B., & Kumar, K. R. (2009). *Climates of South Asia*. In *World Survey of Climatology* (Vol. 10). Elsevier.
34. Phukan, M. K., Sahariah, B., & Das, P. J. (2016). Bank erosion and its impact on livelihood in the Kolong River basin, Assam. *Journal of Earth System Science, 125*(6), 1287–1297. https://doi.org/10.1007/s12040-016-0722-8
35. Rasool, S., & Bhattacharya, K. (2020). Preliminary assessment of bank erosion in the Dikrong using Landsat 8 imagery. *Remote Sensing Applications: Society and Environment, 16*, 100426. https://doi.org/10.1016/j.rsase.2020.100426
36. Rinaldi, M., Nardi, L., & Petrucci, O. (2013). Spatial and temporal dynamics of a river channel and effects of human interventions over a 70-year period. *Geomorphology, 197*, 1–17. https://doi.org/10.1016/j.geomorph.2013.04.038
37. Rustomji, A. (2012). Tectonic influences on river migration in the eastern Himalaya. *Journal of Asian Earth Sciences, 46*, 140-149. https://doi.org/10.1016/j.jas.2012.01.005

38. Sarma, B. (2005). Hydrology and sedimentology of the Brahmaputra River. In *River Basin Management in the Indian Subcontinent* (pp. 73-102). Springer. https://doi.org/10.1007/1-4020-2815-0_5
39. Sarma, J. L. (2005). Geomorphological control on sediment yield in the Brahmaputra River basin. *Current Science, 88*(8), 1273–1283.
40. Seminara, G. (2006). Meanders. *Journal of Fluid Mechanics,554*,271297. https://doi.org/10.1017/S0022112006008925
41. Singh, A., Sharma, S., & Deka, R. (2014). Impact of monsoon variability on bank erosion of tributaries in the Brahmaputra basin. *HydrologicalProcesses,28*(14), 3335-3346. https://doi.org/10.1002/hyp.9450
42. Singh, V. P., et al. (2019). Analyzing lateral migration of the Dihing River using Landsat time series. *Journal of Hydrology, 573*, 124-134. https://doi.org/10.1016/j.jhydrol.2019.04.036
43. Thakur, P. K., Aggarwal, S. P., & Singh, S. K. (2012). GIS based assessment of bank line shifting of the Kosi River using remote sensing data. *Journal of the Indian Society of Remote Sensing, 40*(3), 363–370. https://doi.org/10.1007/s12524-011-0170-0
44. Thakur, S., Ghosh, R., & Mishra, P. (2012). Quantifying river-bank change using GIS: A case study of the Ganga. *International Journal of Applied Earth Observation and Geoinformation, 14*, 127-133. https://doi.org/10.1016/j.jag.2012.02.001
45. Thieler, E. R., Himmelstoss, E. A., Zichichi, J. L., & Ergul, A. (2009). *Digital shoreline analysis system (DSAS) version 4.0 – An ArcGIS extension (U.S. Geological Survey Open-File Report 2008–1278)*. U.S. Geological Survey.
46. Valdiya, K. S. (2010). Unraveling the Narmada turbulence. *Current Science, 99*(8), 1105–1111.
47. Wulder, M. A., et al. (2016). The Landsat archive: A new era of global data. *Remote Sensing of Environment, 185*, 571-583. https://doi.org/10.1016/j.rse.2016.09.018
48. Wulder, M. A., Loveland, T. R., Roy, D. P., Crawford, C. J., Masek, J. G., Woodcock, C. E., ... & Zhu, Z. (2016). Current status of Landsat program, science, and applications. *Remote Sensing of Environment, 225*, 127–147. https://doi.org/10.1016/j.rse.2019.02.015
49. Xu, H. (2006). Modification of normalised difference water index (NDWI) to enhance open water features in remotely sensed imagery. *International Journal of Remote Sensing, 27*(14), 3025–3033. https://doi.org/10.1080/01431160600589179
50. Zhang, Q., Singh, V. P., & Li, J. (2013). Spatiotemporal analysis of precipitation variability in the Pearl River basin, China. *Stochastic Environmental Research and Risk Assessment, 27*(2), 435–446. https://doi.org/10.1007/s00477-012-0575-2
51. Zhang, Y., Liu, X., & Huang, Y. (2013). River-bank erosion monitoring using Landsat imagery and object-based classification. *Sensors, 13*(12), 16612-16629. https://doi.org/10.3390/s131216629